





## Article

# Li-Cs-Na-Rich Beryl from Beryl-Bearing Pegmatite Dike No. 7 of the Shongui Deposit, Kola Province, Russia

Lyudmila N. Morozova <sup>1,2,\*</sup> , Sergey G. Skublov <sup>3,4</sup> , Dmitry R. Zozulya <sup>2</sup> , Pavel A. Serov <sup>2</sup> ,  
Elena S. Borisenko <sup>2</sup>, Anna N. Solovjova <sup>2</sup> and Alexandra K. Gavrilchik <sup>4</sup>

<sup>1</sup> All-Russian Scientific-Research Institute of Mineral Resources Named after N.M. Fedorovsky, 31 Staromonetny Lane, 119017 Moscow, Russia

<sup>2</sup> Geological Institute of the Kola Science Centre of the Russian Academy of Sciences, 14 Fersman St., 184209 Apatity, Russia

<sup>3</sup> Institute of Precambrian Geology and Geochronology of the Russian Academy of Sciences, 2 Makarova Embankment, 199034 St. Petersburg, Russia

<sup>4</sup> St. Petersburg Mining University, Mining Museum, 21st Line 2, 199106 St. Petersburg, Russia

\* Correspondence: morozova@vims-geo.ru

**Abstract:** Beryl is both an accessory and a rock-forming mineral in pegmatites that contain beryl, making it a major source of Be. Beryl-bearing pegmatites of the Shongui deposit, located in the Kola province of the Northeastern Fennoscandian Shield, hold beryl with a yellowish-greenish color. An investigation into the chemical composition of this beryl from pegmatite dike No. 7 has been performed for the first time via the secondary ion mass spectrometry (SIMS) technique, and the chemical composition of the beryl-bearing pegmatites has been analyzed for the first time by the inductively coupled plasma mass spectrometry (ICP-MS) method. These pegmatites have high concentrations (ppm) of Be (11.8), Li (30.9), Rb (482), Nb (50.3), Ta (14.6), Cs (66.8), and Mn (283) and low concentrations of Sr, Y, Ba, rare earth elements (REE), Zr, and Th. In the Shongui pegmatite field, concentrations of Be, Li, Rb, Cs, Nb, Ta, and Mn increase from barren to beryl-bearing pegmatites, whereas concentrations of Ba, Sr, Y, and REE decline. Rb/Ba, Rb/Sr, and Zr/Hf ratios, showing the fractionation degree, change from the barren to beryl-bearing pegmatites: Rb/Ba and Rb/Sr increase from 111 and 0.46 to 1365 and 8.06, respectively, and Zr/Hf decreases from 18.9 to 14.5. The chemical composition of beryl from the Shongui deposit is unique. This mineral has a concentration of 25,300 ppm of alkalis (Li, Cs, K, Rb, Na) and the average Li, Ce, and Na content is 4430, 5000, and 15,400 ppm, respectively. According to its chemical composition, the Shongui beryl belongs to the Li-Cs-Na type, a type that is not recognized in the available classifications. It is supposed that this beryl was mainly crystallized in the magmatic stage rather than in any hydrothermal and metasomatic stages. Two beryl groups have been distinguished in beryl-bearing pegmatite dike No. 7: beryl from the intermediate zone (Brl-I) and beryl from the core zone (Brl-II). These beryls are concluded to have crystallized in the following order: Brl-I and then Brl-II. Compared with Brl-I, Brl-II is depleted in Cs, Na, Cl, and H<sub>2</sub>O and is enriched in Fe and Mn. The Fe/Mn ratio varies from 9.18 to 16.50 in these beryls and their yellowish-greenish shades are thought to be driven by a large amount of Fe compared to Mn.

**Keywords:** beryl; lithium; cesium; granitic pegmatite; Kola province; Shongui deposit; SIMS method



**Citation:** Morozova, L.N.; Skublov, S.G.; Zozulya, D.R.; Serov, P.A.; Borisenko, E.S.; Solovjova, A.N.; Gavrilchik, A.K. Li-Cs-Na-Rich Beryl from Beryl-Bearing Pegmatite Dike No. 7 of the Shongui Deposit, Kola Province, Russia. *Geosciences* **2023**, *13*, 309. <https://doi.org/10.3390/geosciences13100309>

Academic Editors: Micol Bussolesi, Giovanni Grieco, Alessandro Cavallo and Jesus Martinez-Frias

Received: 28 August 2023

Revised: 7 October 2023

Accepted: 13 October 2023

Published: 16 October 2023



**Copyright:** © 2023 by the authors. Licensee MDPI, Basel, Switzerland. This article is an open access article distributed under the terms and conditions of the Creative Commons Attribution (CC BY) license (<https://creativecommons.org/licenses/by/4.0/>).

## 1. Introduction

Beryl is an aluminosilicate mineral of beryllium and is one of main sources of this rare lithophile element. Be is a silvery white and light refractory metal whose alloys with Cu, Al, Mg, Ni, and other metals have unique properties and are widely used in hi-tech industries. These alloys possess elevated hardness, strength, and corrosion resistance and are critical for nuclear power engineering, the electronic industry, the petrochemical sector, the automobile industry, aerospace engineering, and the medical and military industries.

Thus, high-purity Be is a strategic and critical material necessary for the production of national defense facilities.

The history of the discovery and geochemistry of beryl and the value of its ores are discussed in numerous publications [1–13]. In rare metal pegmatites of the lithium-cesium-tantalum (LCT) family (after classification in [14]), beryl is associated with commercially valued minerals of Cs, Li, Nb, and Ta. Nowadays, pegmatites of the LCT family are specifically considered as one of main sources for Be [15–18]. Moreover, beryl is produced from pegmatites of the complex NYF (niobium, yttrium, fluorine)–LCT type (e.g., pegmatites from Anjanabonoina (Madagascar) [19]).

In view of the beryl production, principal pegmatite sites are located in Brazil (Minas Gerais), Portugal (Covas do Barroso pegmatite district), Mozambique (Alto Ligonhain), Canada (Tanco), Namibia (Donkerhoek), Zimbabwe (Bikita, Benson), China (Fujian Province), and Australia (Greenbushes) [12]. Major deposits occur in the USA and are associated with the pegmatite bodies of Kings Mountain (North Carolina), Tin Mountain, and the Black Hills (South Dakota). In Russia, major beryl deposits are known in the Urals (Emerald mines), the Transbaikal region (Adun-Chelon, Sherlovaya Gora), and the Kola Peninsula [18,20].

Another important characteristic of beryl is that its chemical composition provides information on the origin and evolution of granitic pegmatites [10,16,21–27]. Beryl has the ideal formula  $\text{Be}_3\text{Al}_2\text{Si}_6\text{O}_{18}$  but its chemical composition often differs from this due to trace element impurities that occur in the lattice of this mineral [10,21,27–33]. Na, Li, Cs, and Fe along with  $\text{H}_2\text{O}$  can be present in high concentrations [11,34–36]. Trace element impurities also include K, Rb, Mn, V, Cr, Ca, B, F, and some others [2,3,24,27,34,37]. The concentrations of alkali elements, Fe, and Mg together with their ratios in beryl are important in establishing the mineral-forming environments of granitic pegmatites, as well as the differentiation degrees of their parental melts [10,11,21,27,38,39]. The trace element content and mineral, fluid, and melt inclusions in beryl are also used for these purposes [37,40–47]. Meanwhile, some aspects of the crystallization of beryl in different environments and under *P–T* conditions are widely discussed. Contention still exists regarding the impact of the crystal growth conditions and chemical composition on the internal structure and shape of beryl crystals. In addition, some aspects of the classification of this mineral remain incomplete [10,13,26,34,48–50].

Beryl-bearing pegmatites of the Shongui deposit with lithium-tantalum-niobium mineralization are located in the Archean Kola province of the Northeastern Fennoscandian Shield (NW Russia). The internal structure of these pegmatites is well documented [51,52], but the mineralogy and geochemistry of these rocks, along with the geochemistry of the beryl, have not been thoroughly examined. The purpose of this work is to study the chemical composition of the beryl-bearing pegmatites and beryl of the Shongui deposit.

## 2. Geological Setting

The Shongui deposit of beryl-bearing pegmatites was discovered in 1953 and is part of the eponymous pegmatite field located in the Archean Kola-Norwegian terrane of the Kola province [51,52] (Figure 1). The Kola-Norwegian terrane is dominated by tonalite-trondhjemite-granodiorite (TTG) gneisses [53,54], which are intercalated with peraluminous metasedimentary rocks, enderbites, charnockites, and amphibolites. This also contains the Neoarchean Olenegorsk greenstone belt, with deposits of banded iron formations. TTG rocks have an age of 2.8–2.9 Ga and were formed by the partial melting of a mafic lower crust, with pressures varying over a broad range; 2.72–2.63 Ga old granitoids are also present [55–57]. The metasedimentary rocks are interpreted as former mudstones and greywackes. A mature intraplate setting was formed 2.67 Ga ago, and crustal growth continued until ca. 2.6 Ga. An Archean orogeny occurred 2.6–2.8 Ga ago and was followed by the Paleoproterozoic Lapland-Kola collisional orogeny, which took place from ~2.0 to 1.86 Ga [55].

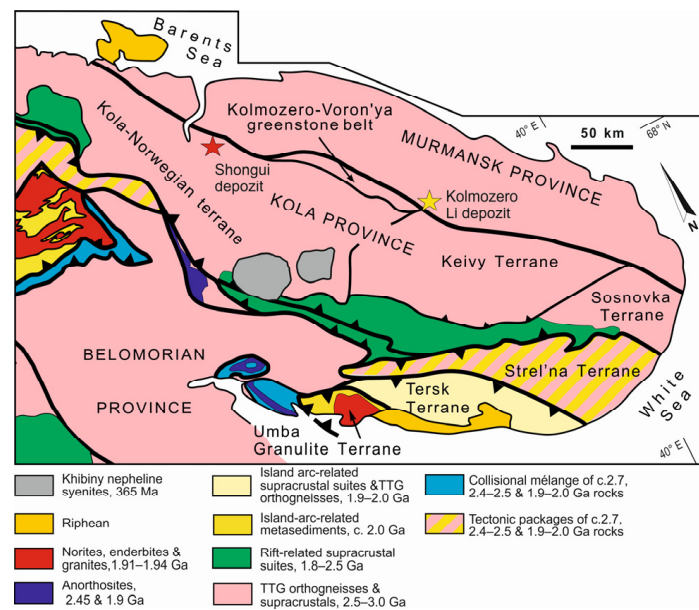


**Figure 1.** Tectonic provinces of the Northeastern Fennoscandian Shield. Modified after Daly et al. [55].

The Shongui pegmatite field holds both beryl-bearing and barren pegmatites (Figure 2), which have been distinguished by mineralogical and structural studies; however, age relationships between these pegmatites remain unclear. The Shongui deposit consists of three dikes of beryl-bearing pegmatites. The best-studied dike (dike No. 7) trends northwest, dipping southwest at an angle of  $45^\circ$ . Beryl from this dike has been chosen as the main object of our study.

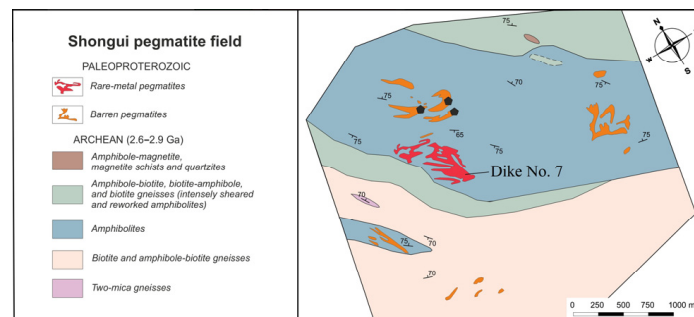


**Figure 2.** Fragment of a schematic map of the Shongui pegmatite field. Black pentagons are a selection site for barren pegmatites.

Beryl-bearing pegmatite dike No. 7 is 1 km long and 60 to 80 m thick, extends down to a depth of 180 m, and cross-cuts amphibolites. This is composed of the border, intermediate, and central zones (Figure 3). The border zone consists of a 10–15 cm thick quartz-plagioclase aplitic zone and a band 10–20 cm thick composed of a medium-grained quartz-albite-microcline aggregate. Amphibolites that are in direct contact with the border zone contain quartz, albite, biotite, tourmaline, and epidote.

The intermediate zone is composed of (i) medium-grained and coarse-grained K-feldspar ( $\pm$ quartz, albite or muscovite) (quartz-albite-microcline aggregates); (ii) megacrystic blocky K-feldspars ( $\pm$ quartz) (quartz-microcline aggregates); (iii) lamellar albite (cleavelandite) ( $\pm$ quartz) (quartz-cleavelandite aggregates). The central zone is composed of the quartz core ( $\pm$ muscovite or albite) (albite-muscovite-quartz aggregates). All these aggregates are partially replaced with later aggregates almost completely composed of saccharoid albite ( $\pm$ fine-grained quartz or fine flake muscovite).

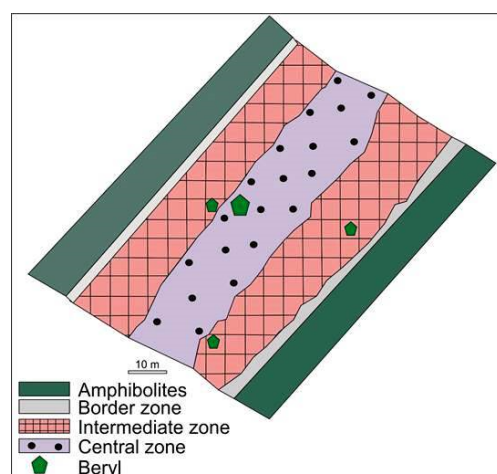


**Figure 3.** Schematic map of the studied part of beryl-bearing pegmatite dike No. 7 of the Shongui deposit.

The main minerals of the beryl-bearing pegmatites are quartz (30–35 vol. %), plagioclase (30–35 vol. %), and K-feldspar (20–25 vol. %). Beryl and spodumene are minor minerals. Accessories include minerals of the columbite group, tourmaline, muscovite, garnet, zircon, apatite, graphite, galena, molybdenite, ilmenite, magnetite, cassiterite, uraninite, and iron and manganese hydroxides [51,52].

The barren pegmatites intrude the amphibolites, biotite, and amphibole-biotite gneisses (Figure 2), have a simple mineral composition, and consist of quartz (35–45 vol. %), K-feldspar (45–60 vol. %), and plagioclase (25–30 vol. %) [51,52].

### 3. Analytical Methods and Samples

#### 3.1. ICP-MS Method

The concentrations of trace elements in the beryl-bearing pegmatite dike No. 7 were determined using inductively coupled plasma mass spectrometry (ICP-MS) on the NexION 300S (PerkinElmer Inc, USA) at the Institute of Geology and Geochemistry UrB RAS (Yekaterinburg, Russia). Ultrapure deionized water filtered using the AriumPro (Sartorius, Germany) system ( $18.2 \text{ M}\Omega \times \text{cm}^{-1}$ ) was used at each stage of the analysis. All the acids applied ( $\text{HNO}_3$ ,  $\text{HCl}$ ,  $\text{HF}$ ) were extra-distilled under a temperature below boiling point (sub-boiling distillation). The operation mode of the NexION 300S mass spectrometer for the multi-element analysis of the sample was as follows: radiofrequency oscillator capacity—1300 W, cone interface material—platinum. All measurements were conducted using quantitative analysis with calibration curves constructed. Multi-element standard solutions (PerkinElmer Instruments) certified according to ISO 9001 standard (<https://www.iso.org/iso-9001-quality-management.html> accessed on 6 October 2023) were used to construct calibration curves. To control the accuracy and precision of the microelement composition detection, certified samples of basalt BCR-2 and andesite AGV-2 (USGS) were used. The obtained concentrations of rare elements, including rare earth elements, complied with the attested values with acceptable variation of 15%.

#### 3.2. SIMS Technique

The content of trace and minor elements, water, and volatiles in beryl was determined by secondary ion mass spectrometry (SIMS) using a Cameca IMS-4f ion microprobe (CAMECA, Gennevillier, France) at the Yaroslavl Branch of the Institute of Physics and Technology (IPT) named after K.A. Valiev, Russian Academy of Sciences. The basics of the measurement techniques corresponded to those described in detail in [46,58–62]. Below, we report only some important information. Calibration curves were determined on the measurements of the set of standard samples [63,64]. Calibrations were obtained using samples of natural and artificial glasses that covered a wide range of variation in  $\text{SiO}_2$  (41.00–77.00 wt. %) and water (0.1–8 wt. %) concentrations [65–69] (unpublished data by



R.E. Bocharnikov). The maximal deviation from the reference value did not exceed 15%, and the calculation error was 7%. A similar approach was used to calculate fluorine and chlorine concentrations, which were determined using standard glass NIST-610 [70] as a monitor before an analytical session.

Petrographic studies were carried out with an Axioplan-2 Imaging Microscope equipped with a digital camera and an image processing system (Carl Zeiss MicroImaging GmbH, Goettingen, Germany) at the Geological Institute KSC RAS.

### 3.3. Samples

Samples of the quartz-albite-microcline, quartz-microcline, and quartz-cleavelandite aggregates were taken from the intermediate zone and samples of the albite-muscovite-quartz aggregates from the central zone of beryl-bearing pegmatite dike No. 7 (Figure 3). For comparison, barren pegmatites were also sampled from three dikes that occur in amphibolites northwest of dike No. 7 (Figure 2). For comparison, we took trench samples across barren pegmatite dikes that occur in amphibolites northwest of dike No. 7. In total, 12 samples of beryl-bearing pegmatites and three samples of barren pegmatites were taken. The weight of samples varied from 20 to 40 kg in dependence on the size of rock-forming minerals.

Beryl samples were gathered from the following aggregates: beryl-I (Brl-Ia) from the quartz-albite-microcline aggregate, beryl-Ib (Brl-Ib) from the quartz-microcline aggregate, beryl-Ic (Brl-Ic) from the quartz-cleavelandite aggregate (Figures 4 and 5a,b), and beryl-II (Brl-II) from the albite-muscovite-quartz aggregate (Figure 5c,d). The size of the beryl crystals varied from 1–2 cm to 0.5 m across. These were characterized by yellowish-green, greenish-yellow, grayish-green, and yellow colors and were transparent and translucent. The beryl crystals contained inclusions of acicular tourmaline, microcrystalline apatite, garnet, quartz, albite, and minerals of the columbite group.

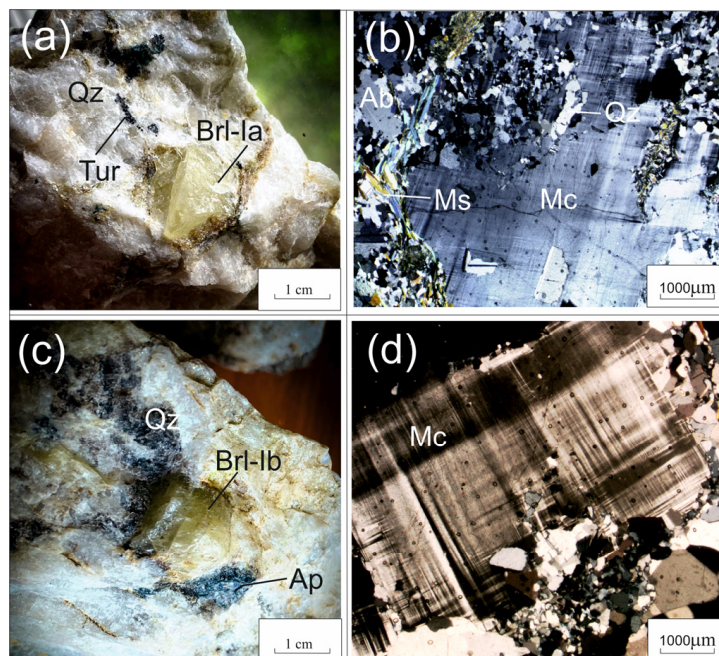


**Figure 4.** Beryl from beryl-bearing pegmatite dike No. 7 of the Shongui deposit. (a) Photograph and (b) photomicrograph (plane polarized light) of greenish-yellow Brl-Ia from the quartz-albite-microcline aggregate; (c) photograph and (d) photomicrograph (plane polarized light) of yellowish-green Brl-Ib from the quartz-microcline aggregate. Ab, albite; Brl, beryl; Mc, microcline; Ms, muscovite; Qz, quartz; Ap, apatite.

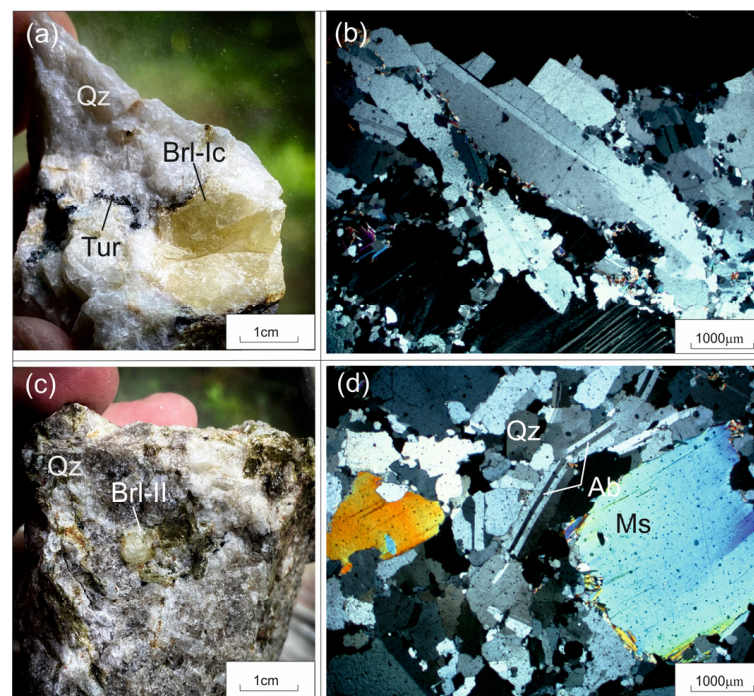


**Figure 5.** Beryl from beryl-bearing pegmatite dike No. 7 of the Shongui deposit. (a) Photograph and (b) photomicrograph (plane polarized light) of yellow Brl-Ic from the quartz-cleavelandite aggregate; (c) photograph and (d) photomicrograph (plane polarized light) of grayish-green Brl-II from the albite-muscovite-quartz aggregate. Ab, albite; Brl, beryl; Mc, microcline; Ms, muscovite; Qz, quartz; Tur, tourmaline.

## 4. Results

### 4.1. Geochemistry of the Beryl-Bearing Pegmatites

Data on the concentrations of rare elements in the quartz-albite-microcline, quartz-microcline, quartz-cleavelandite, and albite-muscovite-quartz aggregates are given in Table 1.

The maximal average Be content was established in the albite-muscovite-quartz (25.3 ppm) and quartz-cleavelandite (19.9 ppm) aggregates. The Be content was 0.77 ppm in the quartz-microcline aggregates and 1.07 ppm in the quartz-albite-microcline aggregates. The Li content varied from 7 to 90 ppm, while the Ce content varied from 3.5 to 223 ppm. The Mn content varied from 27 to 1400 ppm. The maximal average concentrations of Rb (1667 ppm), Cs (223 ppm), Ta (8.67 ppm), and Pb (23.7 ppm) were determined in the quartz-microcline aggregates. The quartz-albite-microcline aggregates had the lowest average concentrations of Li (7.0 ppm), Nb (1.60 ppm), Ta (0.18 ppm), Cs (4.33 ppm), and Ta (0.27 ppm).

The Nb content ranged from 1.5 to 250 ppm, while the Ta content varied from 0.15 to 54 ppm. The average Nb content in the albite-muscovite-quartz (158 ppm) and quartz-cleavelandite (36.7 ppm) aggregates was higher than the Nb content in the quartz-microcline (5.43 ppm) and quartz-albite-microcline (1.60 ppm) aggregates. The Ta distribution showed a similar trend. The Ta content was, on average, 36.3 and 14.8 ppm in the albite-muscovite-quartz and quartz-cleavelandite aggregates, respectively, whereas, in the quartz-microcline and quartz-albite-microcline aggregates, these were 7.07 and 0.18 ppm, respectively.

**Table 1.** Trace elements (ppm) in beryl-bearing pegmatites of dike No. 7 of the Shongui deposit.

	Shongui Deposit												Shongui Pegmatite Field		
Aggregate	Quartz-Albite-Microcline			Quartz-Microcline			Quartz-Cleavelandite			Albite-Muscovite-Quartz			Barren Pegmatites		
Sample	SH-31-1	SH-39-1	SH-116-2	SH-30-1-GH	SH-30-18	SH-30-2-GH	SH-6-GH	SH-111-13	SH-6-GX	SH-30-19	SH-30-23	SH-30-24	L-43-1	L-45-1	A-51-1
Li	7.0	7.0	7.0	17	17	60	15.0	90.0	10.0	60.0	31.0	50.0	1.50	2.90	40.0
Be	1.0	1.1	1.1	0.80	0.80	0.70	2.30	55	2.30	25.0	28.0	23.0	0.70	0.60	1.90
Sc	8.0	2.0	4.1	3.4	2.3	3.7	6.0	11	7.0	1.2	0.7	1.3	3.6	6.0	2.3
Ti	40	40	21	12	21	11	30	30	18	70	30	50	100	60	100
V	1.3	0.26	0.29	0.40	0.41	0.23	0.33	3.0	1.40	0.50	0.60	0.50	2.00	1.70	0.50
Cr	11	16	110	9.0	9.0	9.0	15	110	130	17	17	18	11	16	9
Mn	80	219	90	30	27	29	80	1400	70	380	210	800	40	90	80
Co	0.9	1.2	0.7	0.6	0.4	0.6	1.10	0.80	1.00	1.10	1.20	1.00	1.50	1.40	0.90
Ni	21	31	8.0	16	9.0	15	30	9.0	16	30	34	29	23	28	20
Cu	5.0	7.0	5.0	7.0	3.9	5.0	8.0	8.0	7.0	10.6	8.0	7.0	9.0	9.0	5.0
Zn	9.0	12	6.0	5.0	4.0	6.0	8.0	12	5.0	70	14	20	10	8.0	14
Ga	10	10	12	13	13	14	12	24	11	16	8.0	18	9.0	9.0	13
Ge	1.30	1.20	1.30	2.7	2.7	3.0	1.90	3.00	1.70	2.20	2.10	2.50	0.90	1.00	1.50
As	4.90	22.60	5.30	23.3	24.1	25.5	7.00	9.70	7.70	22.20	21.40	24.10	3.50	4.40	4.30
Se	0.69	0.13	0.09	0.12	0.08	0.15	0.09	b.d.l.	0.07	b.d.l.	b.d.l.	0.08	0.16	0.17	0.14
Rb	73	69	48	1400	1700	1900	61	15	22	120	130	250	48	61	37
Sr	60	70	60	60	60	60	60	60	70	60	50	60	130	130	70
Y	1.4	5.0	1.7	0.11	0.30	0.06	4.00	1.90	1.10	1.30	0.60	1.50	6.00	7.00	5.00
Zr	11	32.8	11	2.4	1.3	1.1	9.0	18	2.20	5.0	7.0	69	29.80	36.60	15
Nb	1.50	1.10	2.20	3.8	1.5	11	5	100	5.0	170	53	250	0.6	0.23	0.4
Mo	1.30	1.70	1.10	0.8	0.6	0.8	1.80	1.10	1.70	1.60	1.80	1.60	1.20	1.50	1.10
Ag	0.12	0.12	0.19	0.14	0.08	0.3	0.19	2.60	0.18	4.20	1.30	6.10	0.06	0.06	0.05
Cd	0.04	0.14	0.06	0.05	0.06	0.06	0.09	0.7	0.07	0.50	0.20	0.90	0.03	0.05	0.07
Sn	2.60	2.50	3.0	2.4	1.3	1.1	4.0	2.10	1.50	22	12	38	0.60	0.60	0.90
Sb	0.09	0.10	0.09	0.22	0.22	0.26	0.19	0.16	0.14	0.26	0.24	0.28	0.07	0.24	0.06
Te	0.06	b.d.l.	b.d.l.	b.d.l.	b.d.l.	0.02	b.d.l.	b.d.l.	b.d.l.	b.d.l.	b.d.l.	0.02	b.d.l.	b.d.l.	b.d.l.
Cs	4.1	5.4	3.5	150	270	250	17	18	10	20	23	30	2.1	3.5	4.4
Ba	14	22	9.0	30	18	18	18	18	16	20	16	40	250	240	80
La	0.80	2.50	0.90	0.20	0.28	0.12	1.40	1.0	1.0	1.70	0.50	2.90	4.0	6.0	6.0
Ce	1.70	6.0	1.80	0.28	0.47	0.18	2.70	1.70	1.90	3.0	1.0	5.0	9.0	13	11
Pr	0.18	0.60	0.20	0.04	0.06	0.02	0.31	0.18	0.20	0.27	0.10	0.40	1.10	1.50	1.20
Nd	0.58	1.90	0.62	0.11	0.28	0.06	0.96	0.47	0.60	0.61	0.29	0.84	3.70	5	3.90
Sm	0.23	0.80	0.29	0.03	0.08	0.01	0.45	0.25	0.24	0.28	0.11	0.27	1.20	1.50	1.30
Eu	0.04	0.05	0.04	0.02	0.04	0.01	0.03	0.01	0.02	0.02	0.01	0.07	0.34	0.31	0.05
Gd	0.26	1.0	0.34	0.03	0.09	0.02	0.56	0.25	0.24	0.26	0.11	0.26	1.50	1.70	1.30
Tb	0.06	0.21	0.07	0.01	0.01	0.02	0.13	0.06	0.05	0.06	0.02	0.05	0.27	0.30	0.21
Dy	0.33	1.20	0.40	0.02	0.04	0.01	0.70	0.37	0.26	0.29	0.12	0.25	1.60	1.70	1.10
Ho	0.05	0.19	0.06	0.00	0.01	0.00	0.10	0.05	0.04	0.03	0.02	0.03	0.27	0.29	0.16

Table 1. Cont.

Aggregate	Shongui Deposit												Shongui Pegmatite Field		
	Quartz-Albite-Microcline			Quartz-Microcline			Quartz-Cleavelandite			Albite-Muscovite-Quartz			Barren Pegmatites		
Sample	SH-31-1	SH-39-1	SH-116-2	SH-30-1-GH	SH-30-18	SH-30-2-GH	SH-6-GH	SH-111-13	SH-6-GX	SH-30-19	SH-30-23	SH-30-24	L-43-1	L-45-1	A-51-1
Er	0.16	0.50	0.16	0.01	0.03	0.00	0.28	0.14	0.1	0.07	0.05	0.06	0.70	0.80	0.44
Tm	0.03	0.08	0.03	0.01	0.02	0.01	0.05	0.03	0.02	0.01	0.01	0.01	0.10	0.11	0.08
Yb	0.23	0.60	0.23	0.01	0.02	0.00	0.40	0.30	0.15	0.08	0.06	0.08	0.60	0.70	0.50
Lu	0.03	0.09	0.03	0.00	0.00	0.00	0.05	0.04	0.02	0.01	0.01	0.01	0.09	0.10	0.07
Hf	0.70	1.80	0.70	0.03	0.04	0.07	0.60	2.10	0.15	0.50	0.40	7.0	1.50	1.80	0.90
Ta	0.15	0.17	0.21	2.5	0.7	18	5.0	37	2.50	41	14	54	0.42	0.07	0.22
W	1.60	2.0	1.50	0.9	0.5	0.7	1.80	1.70	1.0	2.50	2.10	3.20	1.30	1.50	1.10
Tl	0.30	0.30	0.20	7	9	10	0.32	0.07	0.11	0.50	0.60	0.90	0.18	0.21	0.19
Pb	6.0	6.0	6.0	26	21	24	7.0	2.1	7.0	2.0	1.7	1.8	14	19	10
Bi	0.04	0.11	0.06	0.41	0.21	1.4	0.90	0.36	0.24	0.37	0.32	0.30	2.0	1.40	0.14
Th	0.52	2.20	0.80	0.07	0.07	0.1	1.20	0.52	0.60	0.65	0.26	1.90	3.60	5.0	5.0
U	0.90	3.90	1.20	0.14	0.19	0.31	1.20	2.80	0.24	9.0	1.10	5.0	2.30	3.70	1.30

b.d.l.—below detection limit.



All the aggregates were depleted in Ba (9–40 ppm), Sr (50–70 ppm), Y (0.06–1.9 ppm), and REE (0.45–15.7 ppm). Meanwhile, the beryl-bearing pegmatites taken as a whole were depleted in Ni, Cr, Co, Se, Cd, Te, Bi, Th, and V, with concentrations of these elements being less than 1 ppm.

The beryl-bearing pegmatites demonstrate a negative slope of REE patterns ( $(La/Lu)_n = 2.60\text{--}33.47$ ) (Figure 6) and have light REE/heavy REE (LREE/HREE) ratios, which vary from 3.07 to 12.64. The quartz-microcline aggregate shows a positive Eu anomaly ( $Eu/Eu^* = 1.29\text{--}2.19$ ), which is related to the high content of the microcline. Negative Eu anomalies ( $Eu/Eu^* = 0.17\text{--}0.81$ ) are typical of the quartz-albite-microcline, quartz-cleavelandite, and albite-muscovite-quartz aggregates. In the beryl-bearing pegmatites, the fractionation degree of HREE ( $(Gd/Lu)_n$ ) ranges from 0.78 to 4.92, while that of LREE ( $(La/Sm)_n$ ) varies from 1.95 to 6.76. Compared with the highly evolved albite-spodumene pegmatites of the Kolmozero Lithium Deposit (Figure 1) [18,71], these rocks have a higher value of the fractionation index ( $Zr/Hf$  [72]) (14.6 and 6.12, respectively).

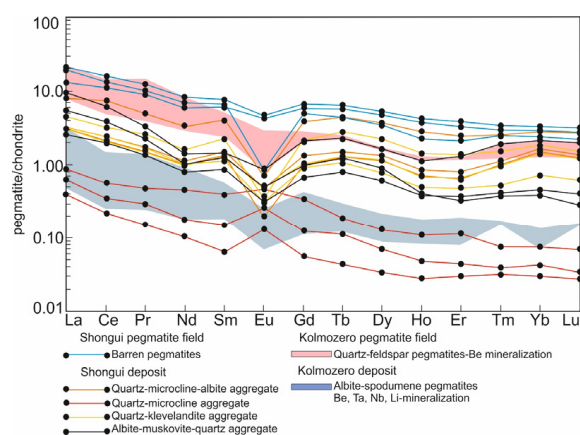


**Figure 6.** Chondrite-normalized [73] REE distribution in the beryl-bearing pegmatites of the Shongui pegmatite field. For comparison, albite-spodumene pegmatites (green field) and quartz-feldspar pegmatites (pink field) of the Kolmozero pegmatite field are shown; data after Morozova [18].

#### 4.2. Geochemistry of the Barren Pegmatites

Compared to the beryl-bearing pegmatites, the barren pegmatites show lower concentrations (ppm) of Li (14.8), Be (1.07), Rb (48.7), Nb (0.41), Cs (3.33), Ta (0.24), Mn (70.0), Sn (0.70), Cr (12.0), and As (4.07), and elevated concentrations (ppm) of Ti (86.7), Sr (110), Y (6.00), Ba (190), Pb (14.3), REE (28.3), Zr (27.1), and Th (4.53). The REE patterns demonstrate a slight negative slope ( $(La/Lu)_n = 4.62\text{--}8.90$ ) and negative Eu anomalies ( $Eu/Eu^* = 0.13\text{--}0.77$ ). The fractionation degree of HREE ( $(Gd/Lu)_n$ ) slightly varies from 2.07 to 2.31 and that of LREE ( $(La/Sm)_n$ ) from 2.10 to 2.90 (Figure 6). The LREE/HREE ratio changes also slightly, from 5.10 to 5.68. The content of light, medium, and heavy REE decreases from the barren to beryl-bearing pegmatites. The barren pegmatites have an average fractionation index ( $Zr/Hf$ ) of 18.9, which is higher than in the beryl-bearing pegmatites (14.6).

#### 4.3. Geochemistry of Beryl

##### 4.3.1. Large-Ion Lithophile Elements (LILE)

Large-ion lithophile elements occur both in beryl lattice sites and in channels between rings of silicon oxide tetrahedra [42]. Among alkali elements, the Na content is highest (15,400 ppm; hereafter, the value is provided as a mean for an analysis set) (Table 2). The Na content in Brl-II (13,200 ppm) is lower than in Brl-Ia (16,400 ppm), Brl-Ib (16,900 ppm), and Brl-Ic (15,100 ppm). Furthermore, this increases from the crystal core towards the rim; for example, the Na content in Brl-Ib is 12,600 ppm in the core and 19,200 ppm at the rim. The same increase in the Na content is common in other grains, in which cores and rims were analyzed.

**Table 2.** Trace elements in beryl (ppm) from the beryl-bearing pegmatite dike No. 7.

Element	Brl-Ia, Spot SH-39-1			Brl-Ib, Spot SH-30-1-GX			Brl-Ic, Spot SH-6-GX			Brl-II, Spot SH-30-23		
	Core	Rim	Intermediate Zone	Core	Rim	Intermediate Zone	Core	Rim	Intermediate Zone	Core	Rim	Intermediate Zone
P	b.d.l.	16.9	8.63	72	123	57.1	93.4	n.d.	55.6	n.d.	3.69	83.9
Ca	77.1	106	108	41.8	135	115	121	91.7	129	136	133	127
Sc	7.11	7.05	7.82	8.76	7.77	7.30	4.10	4.36	7.06	5.48	5.16	5.58
Cr	28.8	32.4	34.7	15.3	40.9	31.8	50.0	22.4	41.8	37.9	32.5	28.9
Ni	184	189	240	125	341	233	370	146	280	198	208	176
Rb	147	137	146	192	163	164	154	152	131	154	178	186
Sr	0.56	0.71	0.85	0.43	0.93	0.88	0.74	0.63	0.70	0.85	0.79	0.73
Cs	6300	7210	4400	5820	6000	6000	6530	7380	3430	2540	3940	2750
Ga	10.6	10.4	12.4	14.1	12.9	12.1	11.9	11.8	12.5	12.1	10.9	12.7
Mn	91.9	88.5	102	70.6	80.2	82.2	84.3	78.9	106	95.9	93.5	132
V	2.95	3.28	3.23	2.41	3.58	3.56	2.64	2.56	2.77	2.35	2.88	2.43
Ti	9.58	13.8	8.78	10.3	12.7	15.3	8.85	7.27	8.62	10.7	7.81	10.8
K	218	272	392	287	317	259	306	280	330	343	351	341
Mg	55.7	53.5	81.4	32.8	52.4	46.5	43.7	30.6	98.2	53.7	45.5	121
Na	15,200	18,600	15,500	12,600	19,200	18,800	15,000	16,100	14,100	12,400	15,000	12,300
Fe	1130	1090	1670	766	951	1020	774	783	1750	1370	1180	1350
Co	1.76	1.66	1.91	1.85	2.56	1.82	2.21	1.25	1.84	1.58	1.71	1.59
B	0.62	0.61	1.12	0.73	0.48	0.62	0.54	0.65	0.98	0.55	0.55	0.40
Li	4750	5660	4090	4350	5610	2180	4770	5380	4080	3870	4450	3920
H <sub>2</sub> O	38,800	38,600	36,900	37,200	39,800	34,300	39,500	40,100	39,300	37,700	39,900	35,500
F	7.25	12.1	11.6	7.39	9.09	12.9	10.4	12.2	6.68	7.00	12.7	7.63
Cl	9200	11,500	8850	8400	11,900	12,800	8810	10,300	7790	7830	9000	7700
Fe/(Mn+Cr+V)	9.11	8.79	11.9	8.67	7.63	8.68	5.65	7.54	11.6	10.1	9.18	8.26

b.d.l. below detection limit; n.d., not determined.

Beryl is characterized by high Cs content (5000 ppm; hereafter, the value is provided as the mean). Within the Brl-I group, the Ce content increases from Brl-Ia (5350 ppm) to Brl-Ib (5940 ppm) and then decreases from Brl-Ib to Brl-Ic (5780 ppm); meanwhile, the Ce content in Brl-II (3080 ppm) is remarkably lower than in any Brl-I variety. In Brl-Ib crystals, the Cs content at the rims is slightly higher than that in the core (6000 and 5820 ppm, respectively). Some of the beryl crystals also display increased Cs content at the rims.

The Li content is fairly high (4430 ppm). Li is considered to occur not only in channels of the beryl lattice, but also at the octahedral position Y replacing Al [74,75] or at the tetrahedral position replacing Be [76]. The highest Li concentrations are observed in Brl-Ia (4830 ppm) and Brl-Ic (4740 ppm). In Brl-Ib and Brl-II, the Li content is comparable (4050 and 4080 ppm, respectively). The Li content increases from the core to rim in all analyzed beryl crystals.

The K content is 308 ppm on average and decreases from Brl-Ia (294 ppm) to Brl-Ib (288 ppm) and then increases for Brl-Ic (305 ppm) and Brl-II (345 ppm). Within one crystal, the K content can be both increasing (in three cases) and decreasing towards the rims. In general, the Ca content (97.2 ppm) correlates with the K content. The Rb content is fairly consistent in all beryl samples (159 ppm). No correlation with geochemically related elements has been established. The Sr abundance is extremely low (0.73 ppm).

Apart from LILE, molecules of the H<sub>2</sub>O and/or OH group, as well as Cl and F, can occur in channels in the beryl lattice. The measured H<sub>2</sub>O content is 38,100 ppm on average. Notably, the H<sub>2</sub>O content rises towards the rim in three samples (except Brl-Ia, in which it remains unchanged).

Beryl has markedly high Cl content (9500 ppm). Brl-II shows the lowest average concentrations of Cl (8177 ppm). The average Cl concentrations in Brl-Ia (9850 ppm), Brl-Ib (11,000 ppm), and Brl-Ic (8970 ppm) are higher than in Brl-II. The Cl content increases from the crystal core to the rim in all samples. The F content is fairly low and varies from 6.68 to 12.9 ppm (9.74 ppm). However, this element tends to increase towards the crystal rim in all samples.

#### 4.3.2. Transition Metals

These elements, including Fe, substitute Al in the octahedral position Y [74,76]. The Fe impurity is most significant, and its content varies from 766 to 1750 ppm (1150 ppm on average). Fe is distributed irregularly within a grain.

Other transition metals are present in far smaller amounts. The Ni content is 224 ppm. Beryl-II (194 ppm) contains less Ni than the other samples of Brl-I. Cr shows a positive correlation with Ni (correlation coefficient,  $r^2 = 0.91$ ). The average Cr content is 33.1 ppm in all analyzed beryls. In each sample, the average Cr content is at the same level. Within grains, no regular variations in the Cr abundance have been determined.

Mn shows a positive correlation with Fe ( $r^2 = 0.72$ ). Its average content is 92.2 ppm. No zonal distribution has been observed within one grain. Mg also shows a strong correlation with Fe ( $r^2 = 0.76$ ), and its average content is 59.6 ppm. Notably, Brl-II shows higher Mg content than any varieties of Brl-I (73.5 ppm).

The content of transition elements such as Ti, Sc, V, and Co is fairly low (10.4, 6.46, 2.89, and 1.81 ppm, respectively). The content of Ga, a rare “twin” element of Al, is 12.0 ppm on average. Its distribution is not zonal and varies in a narrow range of 10.4 to 14.1 ppm. In the beryl lattice, B and P replace Si in the tetrahedron [76]. The B content is minor, about 0.65 ppm, and remains constant in all grains.

The average content of Li, Ce, and Na in beryl from the beryl-bearing pegmatites is 4430, 5000, and 15,400 ppm, respectively. Brl-II from the central zone, compared with Brl-I from the intermediate zone, is depleted in Cs, Na, Cl, and H<sub>2</sub>O and is enriched in Mn and Fe (Table 2).

The iron content in all beryl varieties of the Shongui deposit is higher than the Mn content, and the Fe/Mn ratio varies from 9.18 to 16.50. The beryl color is controlled mainly by the composition of impurities, i.e., chromophores, which include Fe<sup>2+</sup> and Fe<sup>3+</sup> (yellow,

green, and blue color) and  $\text{Mn}^{2+}$  and  $\text{Mn}^{3+}$  (pink, red, and emerald green color) [2,10,39]. The color of the Shongui beryl encompasses yellowish-greenish tones. Therefore, the color of this beryl is thought to be controlled by the content of such impurities, or chromophores, as  $\text{Fe}^{2+}$  and  $\text{Fe}^{3+}$ .

## 5. Discussion

### 5.1. Beryl Classification

Several classifications of beryl have been developed [2,3,21,34,38]. At the earlier stages of beryl studies, varieties of this mineral were distinguished based on its color, transparency, and, rarely, shape. Widely spread is the classification based on alkali impurities (Na, Li, Cs, Rb, K), which enter into the beryl lattice. For the first time, the significance of the occurrence of alkalis in beryl (first of all, Na, Li, and Cs) was reported by Penfield [77]. In dependence on concrete alkali metals and their abundances, the following varieties of beryl are distinguished [2,3,38]:

- alkali-free beryl—the amount of alkalis ( $\text{R}_2\text{O}$ )  $\leq 0.5\%$ ;
- sodium beryl—the amount of alkalis ( $\text{R}_2\text{O}$ )  $> 0.5\%$ ;
- Na-Li beryl—the amount of alkalis ( $\text{R}_2\text{O}$ )  $> 1\%$ ;
- Li-Cs beryl—the amount of alkalis ( $\text{R}_2\text{O}$ )  $> 1\%$ ,
- where R = Na, Li, Cs, Rb, and K.

In the beryl from the beryl-bearing pegmatites of the Shongui deposit, the content of the impurity trace elements is arranged in the following order:  $\text{Na} \gg \text{Cs} > \text{Li} > \text{K} > \text{Rb}$  (Table 2). Within beryl crystals, the content of alkalis ( $\text{Na} + \text{Cs} + \text{Li} + \text{K} + \text{Rb}$ ) varies from 19,300 to 26,800 ppm in the core, from 19,500 to 27,400 ppm in the intermediate zone, and from 23,900 to 31,900 ppm at the rim. Li, Cs, and Na represent from 97.4 to 98.7 wt.% of the total alkali content. The total content of Li, Cs, and Na varies from 18,800 to 26,300 ppm in the core, from 19,000 to 27,000 ppm in the intermediate zone, and from 23,400 to 31,500 ppm at the rim. Consequently, the Shongui beryl is enriched in Na, Li, and Cs. High content of these alkali metals is a unique characteristic of this beryl. These data make it possible to attribute the Shongui beryl to the Li-Cs-Na type, which is not recognized in the available classifications [2,3,38].

We have compared the trace element compositions of beryl from the Shongui beryl-bearing pegmatites with those of beryl from other pegmatite deposits (unpublished SIMS data of S.G. Skublov and A.K. Gavrilchik and LA-ICP-MS data in [32,78,79]; in total, 49 analyses). According to the concentrations of Li and Cs, the Shongui beryl is comparable to beryl from the Zavitsky deposit (Figure 7) and differs from it by higher content of Na, Cl, Fe, Cr, Ni, and Co (Figures 8 and 9). The Shongui beryl is characterized by high content of Fe, Na, Cr, Co, and Ni in comparison with beryl from other regions of the world. In beryl from other pegmatite deposits, the Cr content does not exceed 10 ppm, while the Cr content in beryl from the Shongui deposit is mainly 30–40 ppm. The difference in the Fe content is even more notable. In the Shongui beryl, the Fe content is mainly higher than 1000 ppm, whereas the Fe content does not exceed 300 ppm in beryl from other pegmatite deposits.

In the Shongui beryl, the Ni content is mainly higher than 150 ppm, while it is less than 30 ppm in beryl from other deposits. The Co content is fairly low; the difference between the beryl from the Shongui deposit and deposits around the world can be easily traced based on this element. The Co content ranges from 1.5 to 2 ppm and higher, whereas this is commonly not higher than 1 ppm in beryl from other deposits.

### 5.2. Environment of Beryl Crystallization

According to the experimental data, the temperature, pressure, and enrichment of a pegmatitic melt by  $\text{SiO}_2$ ,  $\text{Al}_2\text{O}_3$ , alkalis, F, P, and  $\text{H}_2\text{O}$  influence the crystallization of beryl in pegmatites. In a peralkaline melt with high  $\text{SiO}_2$  content, the crystallization of beryl decreases with an increase in temperature and increases with the progressive fractionation and complexity of the melt [10,76]. The threshold saturation of Be of a pegmatitic melt is 30 ppm at temperatures of 400–640 °C [26,80].

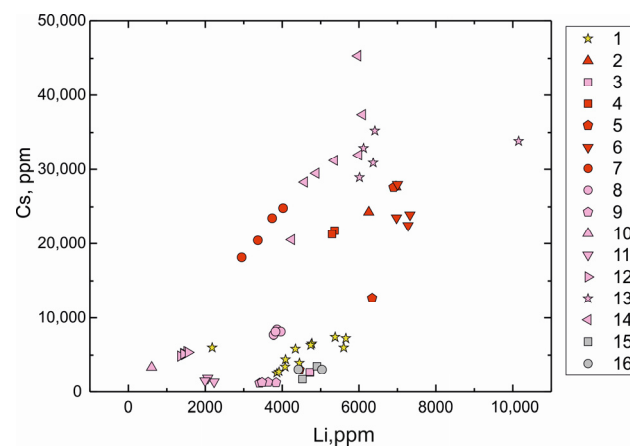


**Figure 7.** Li versus Cs (ppm) plot for beryl from deposits of the world: 1, Shongui deposit, Russia (this study); 2, 6, Elizabeth R, Pala, California, USA; 3, Minas Gerais, Brasilia; 4, Kalba, Eastern Kazakhstan; 5, Madagascar; 7, Shilka region, Transbaikial, Russia; 8, Zavitsinskoye deposit, Transbaikial, Russia; 9, Haapaluoma, Finland; 10, Elba, Italy [32]; 11, Tørdal, Norway [78]; 12, Elba, Italy [79]; 13, Shuk-Byul, Sangilen, Tuva, Russia; 14, Kara-Adyr, Sangilen, Tuva, Russia; 2–9, 13–14, data of S.G. Skublov and A.K. Gavrilchik (13, 14, together with Yu. D. Gritsenko).

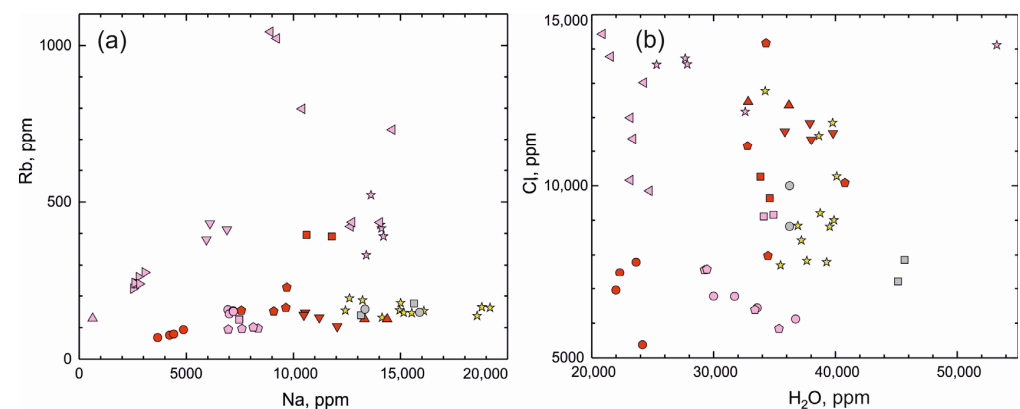


**Figure 8.** (a) Na versus Rb (ppm) plot and (b) H<sub>2</sub>O versus Cl (ppm) plot for beryl from deposits around the world (for symbols, see Figure 7).

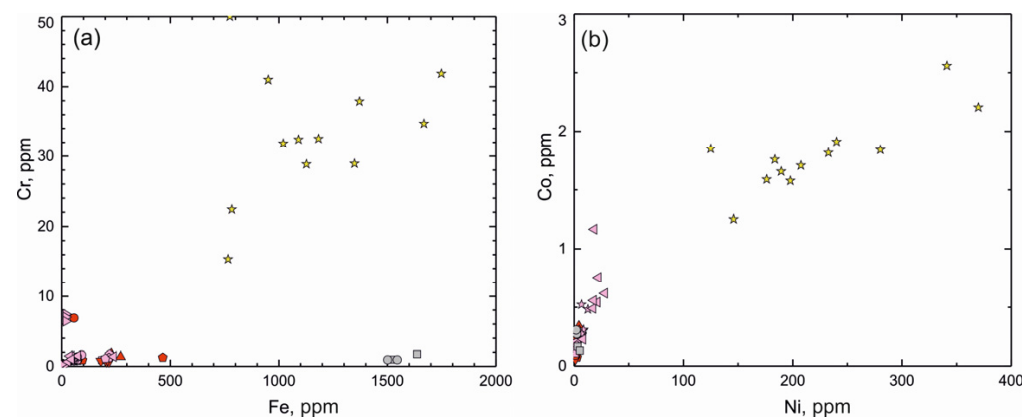


**Figure 9.** (a) Fe versus Cr (ppm) plot and (b) Ni versus Co (ppm) for beryl from deposits around the world (for symbols, see Figure 7).

The Co, Sc, Cr, Ni, Ga, V, and Ti concentrations in beryl from the Shongui deposit are low. In Brl-I and Brl-II, the concentrations of Ga (12 and 12 ppm, respectively) and Sc (6.8



and 5.5 ppm, respectively) are comparable to each other. The content of Ga and Sc has no correlation with other elements and does not provide information about the evolution of the pegmatitic melt.

Some studies have shown that beryl that crystallized at temperatures  $>300\text{ }^{\circ}\text{C}$  is, as a rule, enriched in Ti, Ta, V, and Cr, whereas beryl that crystallized at temperatures of  $200\text{--}300\text{ }^{\circ}\text{C}$  tends to be enriched in Zn and Cu [81]. According to [52], beryl from the Shongui deposit is depleted in Ti, V, and Cr and crystallized at high temperatures of  $415\text{--}460\text{ }^{\circ}\text{C}$  together with feldspars, muscovite, garnet, and tourmaline (plagioclase-alkali-feldspar, muscovite-feldspar, and garnet-tourmaline geothermometers). A high crystallization temperature ( $>300\text{ }^{\circ}\text{C}$ ) is typical for beryl that was formed in the magmatic stage [81]. In the Shongui deposit, Brl-I and Brl-II have average abundances of V (2.9 and 2.6 ppm, respectively), Cr (33 ppm in both varieties), and Ti (10.6 and 9.8 ppm, respectively) and are comparable to each other. Cr shows a positive correlation with Ni ( $r^2 = 0.91$ ) and Co ( $r^2 = 0.56$ ). A positive correlation is also observed between V and Co ( $r^2 = 0.49$ ) and between Ti and Co ( $r^2 = 0.59$ ). In Brl-I and Brl-II, the Co concentrations (1.9 and 1.6 ppm, respectively) are comparable to each other. The Ni content in Brl-II is lower than in Brl-I (194 and 234 ppm, respectively). A positive correlation is observed between Ni and Co ( $r^2 = 0.80$ ).

Brl-I and Brl-II are comparable in their content of F (10 and 9 ppm, respectively) and B (0.7 and 0.5 ppm, respectively), whereas the content of Cl and  $\text{H}_2\text{O}$  is higher in Brl-I (9950 and 38,300 ppm, respectively) than in Brl-II (8180 and 37,700 ppm, respectively). According to [2], the greatest amount of water is characteristic of beryl enriched in alkalis. In addition, gas-liquid inclusions in beryl may contain  $\text{F}^{-1}$ ,  $\text{CO}_3^{2-}$ ,  $\text{SO}_4^{2-}$ , and  $\text{Cl}^{-1}$  [2].

The content of Mg and Mn in Brl-II (74 and 107 ppm, respectively) is higher than in Brl-I (55 and 87 ppm, respectively). Mn shows a positive correlation with Fe ( $r^2 = 0.72$ ) and Mg ( $r^2 = 0.94$ ) and a negative correlation with Cs ( $r^2 = -0.73$ ). Mg also demonstrates a strong correlation with Fe ( $r^2 = 0.76$ ) and a negative correlation with Cs ( $r^2 = -0.66$ ).

### 5.3. Petrogenesis and Evolution of the Pegmatite System

According to the classification of Černý and Ercit based on the mineral and chemical composition [14], the beryl-bearing pegmatites of the Shongui deposit can be referred to as the beryl type that includes moderately fractionated beryl-columbite subtype pegmatites of the LCT (Li-Cs-Ta) family. Beryl can be crystallized at any stage of the formation of pegmatite: (i) at the magmatic stage of crystallization of the marginal, near-wall, and central zones of pegmatites, (ii) during metasomatic processes, or (iii) during late hydrothermal events [2,10].

The Na/Li versus Cs plot for beryl from granitic pegmatites (Figure 10) is used to compare the composition of samples of the Shongui beryl with beryl varieties whose compositions are consistent with the magmatic trend in [10]. Except for one analysis, all data-points of the Shongui beryl fall into the field of magmatic trend, while hydrothermal and metasomatic beryl crystals from other pegmatites do not fall into this field (for example, beryl from the granitic pegmatites of Elba, Italy [39]). Therefore, Brl-I and Brl-II of the Shongui deposit were mainly formed in the magmatic stage.

In beryl, the Cs content and the Cs/Na ratio increase, and the Mg content and the Mg/Fe ratio decrease with the increasing degree of magma differentiation during granitic pegmatite evolution [11,27,82]. In the Brl-I varieties, the Cs content is higher and the Mg content is lower than that in Brl-II. These data suggest that the evolution degree of the quartz-albite-microcline, quartz-microcline, and quartz-cleavelandite zones is higher than that of the albite-muscovite-quartz zone (Figure 11). Rims of beryl crystals from all zones are mainly enriched in Cs (Table 2). As an incompatible element, Cs is commonly accumulated in the residual melt, and its concentration would gradually increase in this melt with the deepening of the magmatic process [83].

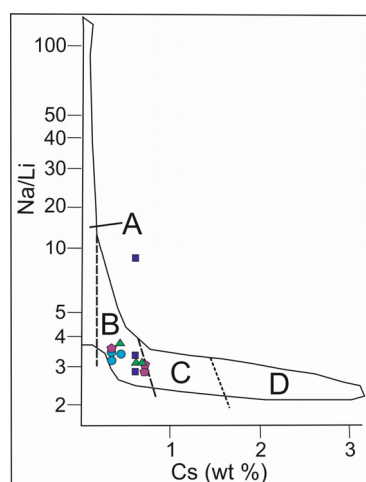


**Figure 10.** Na/Li versus Cs plot for beryl from pegmatites of the Shongui deposit. The magmatic trend according to the pegmatite classification in [10]: (A) barren and geochemically primitive beryl-type pegmatite; (B) geochemically evolved beryl-columbite and beryl-columbite-phosphate pegmatite; (C) albite-spodumene and complex pegmatite; (D) highly fractionated Li, Cs, and Ta-rich complex pegmatite. Green triangle, beryl-1a; dark blue square, Brl-Ib; purple pentagon, Brl-Ic; blue circle, Brl-II.

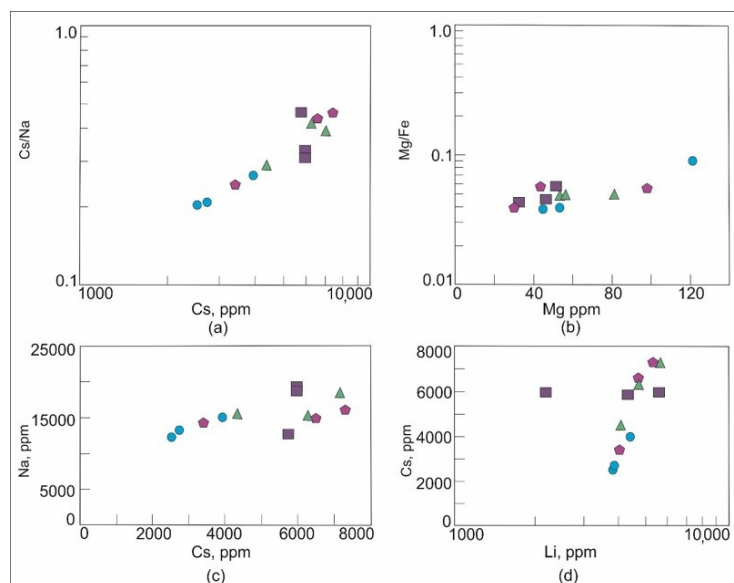


**Figure 11.** Plots (a) Cs/Na versus Cs, (b) Mg/Fe versus Mg, (c) Na versus Cs, and (d) Cs versus Li for beryl of the Shongui deposit. Green triangle, beryl-1a; dark blue square, Brl-Ib; purple pentagon, Brl-Ic; blue circle, Brl-II.

The average concentration of Be, which is an incompatible element, in the barren pegmatites of the Shongui pegmatite field is 1.07 ppm and shows a tendency to increase up to 11.8 ppm in the beryl-bearing pegmatites of the Shongui deposit. From the barren to beryl-bearing pegmatites, the content of incompatible elements such as Li, Rb, and Cs also increases. From the barren pegmatites to beryl-bearing pegmatites, the average content of Cs increases by 20 times, Be by 11 times, Rb by 10 times, Mn by 4 times, Li by 2 times, Ta by 61 times, Tl by 13 times, and Nb by 123 times, whereas the content of Sr, Ba, Y, and REE decreases. The ratios of Rb/Ba, Rb/Sr, and Zr/Hf, showing the fractionation degree, change from the barren to beryl-bearing pegmatites: Rb/Ba and Rb/Sr increase from 111 and 0.46 to 1365 and 8.06, respectively, and Zr/Hf decreases from 18.9 to 14.5 (Figure 12).

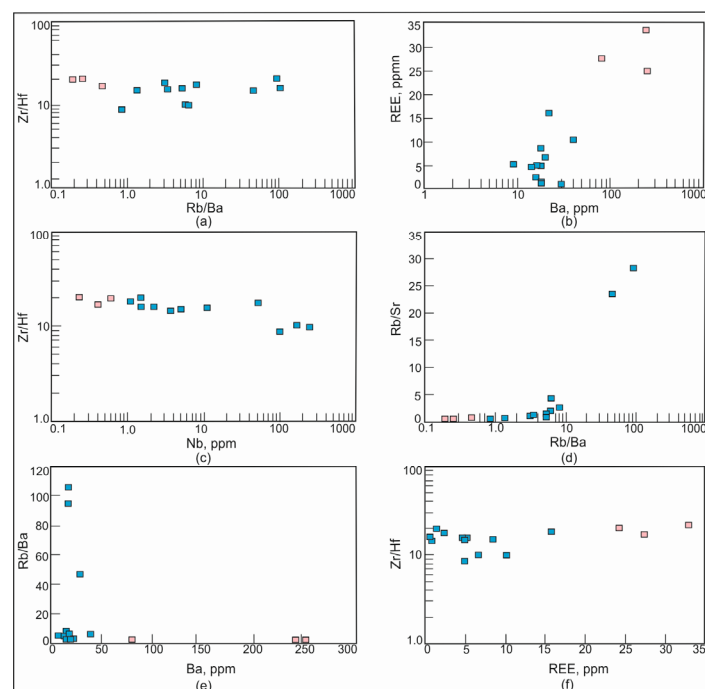


**Figure 12.** Plots Rb/Ba versus Zr/Hf, Ba versus REE, Nb versus Sr/Hf, Rb/Ba versus Rb/Sr, Ba versus Rb/Ba, and REE versus Zr/Hf for pegmatites of the Shongui pegmatite field. Blue square, beryl-bearing pegmatites; pink square, barren pegmatites.

In the pegmatite system, the fractionation of alkali and alkali–earth elements can be caused by (i) fractional crystallization and (ii) hydrothermal processes. Residual melts become progressively enriched in Rb, Li, Be, and Cs and depleted in Sr, Ba, and REE during crystallization. In contrast, Ba and, to a lesser extent, Sr tend to accumulate at the latest stages of hydrothermal processes [7,83]. The distribution of Ba, Sr, and REE confirms the decisive role of fractional crystallization rather than hydrothermal processes in the evolution of the beryl-bearing pegmatite system of the Shongui deposit.

Therefore, the observed trends in the distribution of incompatible elements in the pegmatites of the Shongui pegmatite field suggest that the barren pegmatites were crystallized in the early stages of the formation of this pegmatite field and the beryl-bearing pegmatites at the later stages. Similar trends have been also reported from other regions of the world (for example, [84]).

The geochemical features of pegmatites, including trace element ratios, can indicate the geochemical specialization of pegmatites [85]. Our data show that beryl-bearing pegmatites differ from barren pegmatites in their concentrations of Be, Li, Rb, Cs, Nb, Ta, Mn, Sn, Cr, Sr, Ba, Y, Th, Pb, Ti, Zr, and REE (Table 2).

## 6. Conclusions

1. The chemical composition of beryl from the beryl-bearing pegmatites of the Shongui deposit is unique due to the very high total content of alkalis (Li, Cs, K, Rb, and Na), which is higher than the highest concentrations of Li, Cs, and Na reported from other beryl-bearing pegmatites throughout the world. According to its chemical composition, the Shongui beryl belongs to the Li-Cs-Na type, a type that was not recognized in the available classifications.
2. The content of Be, Li, Rb, Cs, Nb, Ta, and Mn increases, while the content of Ba, Sr, Y, and REE decreases, from the barren to beryl-bearing pegmatites in the Shongui pegmatite field. Respectively, the Rb/Ba, Rb/Sr, and Zr/Hf ratios, showing the fractionation degree, change from the barren to beryl-bearing pegmatites: Rb/Ba and Rb/Sr increase and Zr/Hf decreases.

3. The beryl of the Shongui deposit was mainly formed in the magmatic stage rather than in the hydrothermal and metasomatic stages. The following sequence of crystallization of beryl varieties from beryl-bearing pegmatite dike No. 7 is proposed: at first, Brl-I from the intermediate zone and then Brl-II from the central zone. Compared with Brl-I, Brl-II is depleted in Cs, Li, Na, Ca, Cl, P, Ni, and H<sub>2</sub>O and is enriched in Mn, Mg, and Fe.
4. The color of the Shongui beryl, with yellowish-greenish tones, is controlled by the high Fe content compared to the Mn content.

**Author Contributions:** Conceptualization, L.N.M. and S.G.S.; Methodology, L.N.M., S.G.S. and D.R.Z.; Project administration, L.N.M., S.G.S. and D.R.Z.; Resources, L.N.M.; Visualization, E.S.B., A.N.S. and A.K.G.; Writing—original draft, L.N.M., S.G.S. and P.A.S.; Writing—review and editing, L.N.M., S.G.S. and D.R.Z. All authors have read and agreed to the published version of the manuscript.

**Funding:** This research has been carried out in the framework of the Russian Science Foundation Grant No. 22-17-20002, <https://rscf.ru/project/22-17-20002/> (accessed on 25 March 2022).

**Data Availability Statement:** Data are contained within the article.

**Acknowledgments:** We thank Evgeny Potapov and Sergey Simakin, who assisted with measuring beryl trace and minor element compositions. The authors are grateful to the Mining Museum (St. Petersburg) and Yu. D. Gritsenko (Fersman Mineralogical Museum, Moscow) for the Cs-Li-rich beryl samples kindly provided for analyses. The authors express their gratitude to M.Yu. Sidorov, E.L. Kunakkuzin and I.A. Koval (GI KSC RAS) for their assistance during field work. The manuscript was made clearer and more understandable through constructive criticism from two anonymous reviewers, who are gratefully acknowledged. V.V. Balagansky is highly appreciated for the numerous and useful notes provided on the final version of the manuscript. The authors sincerely thank the editorial team for its assistance.

**Conflicts of Interest:** The authors declare no conflict of interest.

## References

1. Griffith, R.F. Historical Note on Sources and Uses of Beryllium. In *The Metal Beryllium*; White, D.W., Burke, J.E., Eds.; The American Society for Metals: Cleveland, OH, USA, 1955; pp. 5–13.
2. Beus, A.A. *Geochemistry of Beryllium and Genetic Types of Beryllium Deposits*; W. H. Freeman: San Francisco, CA, USA, 1966.
3. Ginzburg, A.I. *The Genetic Types of Hydrothermal Beryllium Deposits*; Nedra: Moscow, Russia, 1975.
4. Gaines, R.V. Beryl—A review. *Mineral. Rec.* **1976**, *7*, 211–223.
5. Hörmann, P.K. Handbook of Geochemistry II/1 Elements H (1)–Al (13). In *Beryllium*; Wedepohl, K.H., Ed.; Springer: Berlin/Heidelberg, Germany, 1978; pp. 1–6.
6. Burt, D.M. Granitic Pegmatites in Science and Industry. In *Minerals of Beryllium*; Černý, P., Ed.; Short Course Handbook 8; Mineralogical Association of Canada: Québec, QC, Canada, 1982; pp. 135–148.
7. Černý, P. Geochemical and petrogenetic features of mineralization in rare-element granitic pegmatites in the light of current research. *Appl. Geochem.* **1992**, *7*, 393–416.
8. Pekov, I.V. Remarkable finds of minerals of beryllium: From the Kola Peninsula to Primorie. *World Ston.* **1994**, *4*, 10–26.
9. Grew, E.S. Mineralogy, Petrology and Geochemistry of Beryllium: An Introduction and List of Beryllium Minerals. *Rev. Mineral. Geochem.* **2002**, *50*, 1–76. [[CrossRef](#)]
10. Černý, P. Mineralogy of beryllium in granitic pegmatites. In *Mineralogy, Petrology, and Geochemistry, Reviews in Mineralogy and Geochemistry*; Grew, E.S., Ed.; Mineralogical Society of America: Washington, DC, USA, 2022; pp. 405–444.
11. Černý, P.; Anderson, A.J.; Tomascak, P.B.; Chapman, R. Geochemical and morphological features of beryl from the Bikita granitic pegmatite, Zimbabwe. *Can. Miner.* **2003**, *41*, 1003–1011. [[CrossRef](#)]
12. Kesler, S.E.; Gruber, P.W.; Medina, P.A.; Keoleian, G.A.; Everson, M.P.; Wallington, T.J. Global lithium resources: Relative importance of pegmatite, brine and other deposits. *Ore Geol. Rev.* **2012**, *48*, 55–69. [[CrossRef](#)]
13. Linnen, R.L.; Van Lichtenvelde, M.; Černý, P. Granitic Pegmatites as Sources of Strategic Metals. *Elements* **2012**, *8*, 275–280. [[CrossRef](#)]
14. Černý, P.; Ercit, T.S. The classification of granitic pegmatites revisited. *Can. Mineral.* **2005**, *43*, 2005–2026. [[CrossRef](#)]
15. London, D.; Kontak, D.J. Granitic Pegmatites: Scientific Wonders and Economic Bonanzas. *Elements* **2012**, *8*, 257–261. [[CrossRef](#)]
16. Sardi, F.G.; Heimann, A. Pegmatitic beryl as indicator of melt evolution: Example from the Velasco district, Pampeana pegmatite province, Argentina, and review of worldwide occurrences. *Can. Mineral.* **2014**, *52*, 809–836. [[CrossRef](#)]

17. Foley, N.K.; Jaskula, B.W.; Piatak, N.M.; Schulte, R.F. Critical Mineral Resources of the United States-Economic and Environmental Geology and Prospects for Future Supply. In *Beryllium*; Schulz, K.J., DeYoung, J.H., Seal, R.R., Bradley, D.C., Eds.; U.S. Geological Survey Professional Paper; U.S. Geological Survey: Reston, VA, USA, 2017; p. 1802. [\[CrossRef\]](#)
18. Morozova, L.N. Kolmozero lithium deposit of rare metal pegmatites: New data on rare element composition (Kola Peninsula). *Lithosphere* **2018**, *18*, 82–98. [\[CrossRef\]](#)
19. Martin, R.F.; De Vito, C. The patterns of enrichment in felsic pegmatites ultimately depend on tectonic setting. *Can. Mineral.* **2005**, *43*, 2027–2048. [\[CrossRef\]](#)
20. Lyalina, L.; Selivanova, E.; Zozulya, D.; Ivanyuk, G. Beryllium Mineralogy of the Kola Peninsula, Russia—A Review. *Minerals* **2018**, *9*, 12. [\[CrossRef\]](#)
21. Aurisicchio, C.; Fioravanti, G.; Grudessi, O.; Zanazzi, P.F. Reappraisal of the crystal chemistry of beryl. *Am. Mineral.* **1988**, *73*, 826–837.
22. Černý, P.; Turnock, A. Beryl from the granitic pegmatites at Greer Lake, Southeastern Manitoba. *Can. Mineral.* **1975**, *13*, 55–61.
23. London, D. *Pegmatites*; The Canadian Mineralogist, Special Publication 10; Mineralogical Association of Canada: Québec, QC, Canada, 2008; pp. 1–347.
24. Bačík, P.; Fridrichová, J.; Uher, P.; Vaculovič, T.; Bizovská, V.; Škoda, R.; Miglierini, M.; Malíčková, I. Beryl crystal chemistry and trace elements: Indicators of pegmatite development and fractionation (Damara Belt, Namibia). *Lithos* **2021**, *404–405*, 106441. [\[CrossRef\]](#)
25. Daneshvar, N.; Azizi, H.; Asahara, Y.; Tsuboi, M.; Minami, M.; Mohammad, Y.O. Geochemistry and Genesis of Beryl Crystals in the LCT Pegmatite Type, Ebrahim-Attar Mountain, Western Iran. *Minerals* **2021**, *11*, 717. [\[CrossRef\]](#)
26. Evensen, J.M.; London, D. Experimental silicate mineral/melt partition coefficients for beryllium, and the beryllium cycle from migmatite to pegmatite. *Geoch. Cosmoch. Acta.* **2002**, *66*, 2239–2265. [\[CrossRef\]](#)
27. Uher, P.; Chudík, P.; Bačík, P.; Vaculovič, T.; Galiová, M. Beryl composition and evolution trends: An example from granitic pegmatites of the beryl-columbite subtype, Western Carpathians, Slovakia. *J. Geosc.* **2010**, *55*, 69–80. [\[CrossRef\]](#)
28. Aurisicchio, C.; Grubessi, O.; Zecchini, P. Infrared spectroscopy and crystal chemistry of the beryl group. *Can. Min.* **1994**, *32*, 55–68.
29. Aurisicchio, C.; Conte, A.M.; De Vito, C.; Ottolini, L. Beryl from miarolitic pockets of granitic pegmatites, Elba, Italy: Characterization of crystal chemistry by means of EMP and SIMS analyses. *Can. Mineral.* **2012**, *50*, 1467–1488. [\[CrossRef\]](#)
30. Fukuda, J.; Shinoda, K. Coordination of water molecules with Na<sup>+</sup> cations in a beryl channel as determined by polarized IR spectroscopy. *Phys. Chem. Miner.* **2008**, *35*, 347–357. [\[CrossRef\]](#)
31. Fukuda, J.; Shinoda, K.; Nakashima, S.; Miyoshi, N.; Aikawa, N. Polarized infrared spectroscopic study of diffusion of water molecules along structure channels in beryl. *Am. Mineral.* **2009**, *94*, 981–985. [\[CrossRef\]](#)
32. Lambruschi, E.; Gatta, G.D.; Adamo, I.; Bersani, D.; Salvioli-Mariani, E.; Lottici, P.P. Raman and structural comparison between the new gemstone pezzottaite Cs(Be<sub>2</sub>Li)Al<sub>2</sub>Si<sub>6</sub>O<sub>18</sub> and Cs-beryl. *J. Raman Spectr.* **2014**, *45*, 993–999. [\[CrossRef\]](#)
33. Kolesov, B.A.; Geiger, C.A. The orientation and vibrational states of H<sub>2</sub>O in synthetic alkali-free beryl. *Phys. Chem. Miner.* **2000**, *27*, 557–564. [\[CrossRef\]](#)
34. Wang, P.; Gray, T.P.; Li, Z.; Anderson, E.J.D.; Allaz, J.; Smyth, J.R.; Koenig, A.E.; Qi, L.; Zhou, Y.; Raschke, M.B. Mineralogical classification and crystal water characterisation of beryl from the W–Sn–Be occurrence of Xuebaoding, Sichuan province, western China. *Min. Mag.* **2021**, *85*, 172–188. [\[CrossRef\]](#)
35. Fukuda, J.; Shinoda, K. Water molecules in beryl and cordierite: High-temperature vibrational behavior, dehydration, and coordination to cations. *Phys. Chem. Miner.* **2011**, *38*, 469–481. [\[CrossRef\]](#)
36. Hawthorne, F.C.; Černý, P. The alkali-metal positions in Cs–Li beryl. *Can. Mineral.* **1977**, *15*, 414–421.
37. Suo, Q.; Shen, P.; Luo, Y.; Li, C.; Feng, H.; Cao, C.; Pan, H.; Bai, Y. Beryl Mineralogy and Fluid Inclusion Constraints on the Be Enrichment in the Dakalasu No.1 Pegmatite, Altai, NW China. *Minerals* **2022**, *12*, 450. [\[CrossRef\]](#)
38. Černý, P. Alkali variations in pegmatitic beryls and their petrogenetic implications. *Neues Jahrb. Min. Abhandl.* **1975**, *123*, 198–212.
39. Neiva, A.; Neiva, J. Beryl from the granitic pegmatite at Namivo, Alto Ligonha, Mozambique. *Neues Jahrb. Mineral. Abhandl.* **2005**, *18*, 173–182. [\[CrossRef\]](#) [\[PubMed\]](#)
40. Bidny, A.S.; Baksheev, I.A.; Popov, M.P.; Anosova, M.O. Beryl from deposits of the Ural Emerald Belt, Russia: ICP-MS-LA and infrared spectroscopy study. *Mosc. Univ. Geol. Bull.* **2011**, *66*, 108–115. [\[CrossRef\]](#)
41. Aurisicchio, C.; Conte, A.M.; Medeghini, L.; Ottolini, L.; De Vito, C. Major and trace element geochemistry of emerald from several deposits: Implications for genetic models and classification schemes. *Ore Geol. Rev.* **2018**, *94*, 351–366. [\[CrossRef\]](#)
42. Giuliani, G.; Groat, L.A.; Marshall, D.; Fallick, A.E.; Branquet, Y. Emerald deposits: A review and enhanced classification. *Minerals* **2019**, *9*, 105. [\[CrossRef\]](#)
43. Saeseaw, S.; Pardieu, V.; Sangsawong, S. Three-phase inclusions in emerald and their impact on origin determination. *Gems Gemol.* **2014**, *50*, 114–132. [\[CrossRef\]](#)
44. Saeseaw, S.; Renfro, N.D.; Palke, A.C.; Sun, Z.; McClure, S.F. Geographic origin determination of emerald. *Gems Gemol.* **2019**, *55*, 614–646. [\[CrossRef\]](#)
45. Zheng, Y.; Yu, X.; Guo, H. Major and trace element geochemistry of Dayakou vanadium-dominant emerald from Malipo (Yunnan, China): Genetic model and geographic origin determination. *Minerals* **2019**, *9*, 777. [\[CrossRef\]](#)



46. Skublov, S.G.; Gavrilchik, A.K.; Berezin, A.V. Geochemistry of beryl varieties: Comparative analysis and visualization of analytical data by principal component analysis (PCA) and t-distributed stochastic neighbor embedding (t-SNE). *J. Min. Inst.* **2022**, *255*, 455–469. [\[CrossRef\]](#)
47. Chen, Z.; Wan, S.; Lu, X.; Wang, W. Study on fluid inclusions in beryl from Pingwu, Sichuan province. *Geol. Sci. Technol. Inf.* **2002**, *21*, 65–73.
48. Thomas, R.; Webster, J.D.; Davidson, P. Be-daughter minerals in fluid and melt inclusions: Implications for the enrichment of Be in granite-pegmatite systems. *Contrib. Mineral. Petrol.* **2011**, *161*, 483–495. [\[CrossRef\]](#)
49. Rao, C.; Wang, R.C.; Hu, H. Paragenetic assemblage of beryllium silicates and phosphates from the Nanping granite pegmatite dyke; Fujian province southeastern China. *Can. Mineral.* **2011**, *49*, 1175–1187. [\[CrossRef\]](#)
50. Schilling, J.; Bingen, B.; Skar, Q.; Wenzel, T.; Markl, G. Formation and evolution of the Høgtuva beryllium deposit, Norway. *Contrib. Mineral. Petrol.* **2015**, *170*, 30. [\[CrossRef\]](#)
51. Antonyuk, E.S. Structural-mineral associations of granite pegmatite veins. In *Materials on Mineralogy of the Kola Peninsula*; CF of the USSR Academy of Sciences: Apatity, Russia, 1962; pp. 134–142.
52. Ponomareva, N.I.; Gordienko, V.V.; Shurekova, R.S. Physico-chemical conditions for the formation of beryl in the Bolshoy Lapot deposit (Kola Peninsula). *Bull. St. Petersburg Univ.* **2005**, *7*, 4–20.
53. Rundqvist, D.V.; Mitrofanov, F.P. (Eds.) *Precambrian Geology of the USSR*; Elsevier Science: Amsterdam, The Netherlands, 1993.
54. Glebovitsky, V.A. (Ed.) *Early Precambrian of the Baltic Shield*; Nauka: Saint-Petersburg, Russia, 2005.
55. Daly, J.S.; Balagansky, V.V.; Timmerman, M.J.; Whitehouse, M.J. The Lapland–Kola orogen: Palaeoproterozoic collision and accretion of the northern Fennoscandian lithosphere. In *European Lithosphere Dynamics, Memoir 32*; Gee, D.G., Stephenson, R.A., Eds.; Geological Society: London, UK, 2006; pp. 579–597.
56. Mints, M.V. Kolmozero-Voronya belt. In *East European Craton: Early Precambrian History and 3D Models of Deep Crustal Structure*; Condie, K., Harvey, F.E., Eds.; Special Paper 510; Geological Society of America: Boulder, CO, USA, 2015; pp. 39–40.
57. Hölttä, P.; Balagansky, V.; Garde, A.A.; Mertanen, S.; Peltonen, P.; Slabunov, A.; Sorjonen-Ward, P.; Whitehouse, M. Archean of Greenland and Fennoscandia. *J. Int. Geosci.* **2008**, *31*, 13–19. [\[CrossRef\]](#) [\[PubMed\]](#)
58. Gavrilchik, A.K.; Skublov, S.G.; Kotova, E.L. Trace Element Composition of Beryl from the Sherlovaya Gora Deposit, South-Eastern Transbaikalia, Russia. *Proc. Russ. Mineral. Soc.* **2021**, *2*, 69–82. [\[CrossRef\]](#)
59. Abdel Gawad, A.E.; Ene, A.; Skublov, S.G.; Gavrilchik, A.K.; Ali, M.A.; Ghoneim, M.M.; Nastavkin, A.V. Trace element geochemistry and genesis of beryl from Wadi Nugrus, South Eastern Desert, Egypt. *Minerals* **2022**, *12*, 206. [\[CrossRef\]](#)
60. Nosova, A.A.; Narkisova, V.V.; Sazonova, L.V.; Simakin, S.G. Minor elements in clinopyroxene from Paleozoic volcanics of the Tagil island arc in the Central Urals. *Geochem. Int.* **2002**, *40*, 219–232.
61. Portnyagin, M.V.; Simakin, S.G.; Sobolev, A.V. Fluorine in primitive magmas of the Troodos Ophiolite Complex, Cyprus: Analytical methods and main results. *Geoch. Int.* **2002**, *40*, 625–632.
62. Portnyagin, M.; Almeev, R.; Matveev, S.; Holtz, F. Experimental evidence for rapid water exchange between melt inclusions in olivine and host magma. *Earth Planet. Sci. Lett.* **2008**, *272*, 541–552. [\[CrossRef\]](#)
63. Jochum, K.P.; Dingwell, D.B.; Rocholl, A.; Stoll, B.; Hofmann, A.W.; Becker, S.; Besmehn, A.; Bessette, D.; Dietze, H.-J.; Dulski, P.; et al. The preparation and preliminary characterisation of eight geological MPI-DING reference glasses for in-situ microanalysis. *Geost. Newsl.* **2000**, *24*, 87–133. [\[CrossRef\]](#)
64. Jochum, K.P.; Stoll, B.; Herwig, K.; Willbold, M.; Hofmann, A.W.; Amini, M.; Aarburg, S.; Abouchami, W.; Hellebrand, E.; Mocek, B.; et al. MPI-DING reference glasses for in situ microanalysis: New reference values for element concentrations and isotope ratios. *Geochem. Geophys. Geosystems* **2006**, *7*, Q02008. [\[CrossRef\]](#)
65. Sobolev, A.V.; Chaussidon, M. H<sub>2</sub>O concentrations in primary melts from island arcs and mid-ocean ridges: Implications for H<sub>2</sub>O storage and recycling in the mantle. *Earth Planet. Sci. Lett.* **1996**, *137*, 45–55. [\[CrossRef\]](#)
66. Danyushevsky, L.V.; Eggins, S.M.; Falloon, T.J.; Christie, D.M. H<sub>2</sub>O abundance in depleted to moderately enriched mid-ocean ridge magmas; Part I: Incompatible behaviour, implications for mantle storage, and origin of regional variations. *J. Petrol.* **2000**, *41*, 1329–1364. [\[CrossRef\]](#)
67. Kamenetsky, V.S.; Everard, J.L.; Crawford, A.J.; Varne, R.; Eggins, S.M.; Lanyon, R. Enriched end-member of primitive MORB melts: Petrology and geochemistry of glasses from Macquarie Island (SW Pacific). *J. Petrol.* **2000**, *41*, 411–430. [\[CrossRef\]](#)
68. Shishkina, T.A.; Botcharnikov, R.E.; Holtz, F.; Varne, R.; Eggins, S.M.; Lanyon, R. Solubility of H<sub>2</sub>O and CO<sub>2</sub>-bearing fluids in tholeiitic basalts at pressures up to 500 MPa. *Chem. Geol.* **2010**, *277*, 115–125. [\[CrossRef\]](#)
69. Tamic, N.; Behrens, H.; Holtz, F. The solubility of H<sub>2</sub>O and CO<sub>2</sub> in rhyolitic melts in equilibrium with a mixed CO–H<sub>2</sub>O fluid phase. *Chem. Geol.* **2001**, *174*, 333–347. [\[CrossRef\]](#)
70. Rocholl, A.B.E.; Simon, K.; Jochum, K.P.; Bruhn, F.; Gehann, R.; Kramar, U.; Luecke, W.; Molzahn, M.; Pernicka, E.; Seufert, M.; et al. Chemical characterisation of NIST silicate glass certified reference material SRM 610 by ICP-MS, TIMS, LIMS, SSMS, INAA, AAS and PIXE. *Geostand. Newslett.* **1997**, *21*, 101–114. [\[CrossRef\]](#)
71. Morozova, L.N.; Sokolova, E.N.; Smirnov, S.Z.; Balagansky, V.V.; Bazai, A.V. Spodumene from rare-metal pegmatites of the Kolmozero lithium world-class deposit on the Fennoscandian shield: Trace elements and crystal-rich fluid inclusions. *Mineral. Mag.* **2021**, *85*, 149–160. [\[CrossRef\]](#)
72. Zaraiskii, G.P.; Aksyuk, A.M.; Devyatova, V.N. The Zr/Hf ratio as a fractionation indicator of rare-metal granites. *Petrology* **2009**, *17*, 25–45. [\[CrossRef\]](#)

73. Boynton, W.V. *Cosmochemistry of the Rare Earth Elements: Meteorite Studies. Rare Earth Element Geochemistry*; Henderson, P., Ed.; Elsevier: Amsterdam, The Netherlands, 1984; pp. 63–114.
74. Staatz, M.H.; Griffitts, W.R.; Barnett, P.R. Differences in the minor element compositions of beryl in various environments. *Am. Mineral.* **1965**, *50*, 1783–1795.
75. Andersson, L.O. The positions of H<sup>+</sup>, Li<sup>+</sup> and Na<sup>+</sup> impurities in beryl. *Phys. Chem. Miner.* **2006**, *33*, 403–416. [[CrossRef](#)]
76. Černý, P.; Hawthorne, F.C. Refractive indices versus alkali contents in beryl: General limitations and applications to some pegmatitic types. *Can. Mineral.* **1976**, *14*, 491–497.
77. Penfield, S.L.; Harper, D.N. On the chemical composition of herderite and beryl, with note on the precipitation of aluminum and separation of beryllium and aluminum. *Am. J. Sci.* **1886**, *32*, 107.
78. Wilhelmsen, M.N. *The Scandium Content of Beryllium-Bearing Minerals and Micas from Tørdal Pegmatites and Its Genetic and Economic Implications*; University of Oslo: Oslo, Norway, 2020.
79. Caucia, F.; Marinoni, L.; Callegari, A.M.; Leone, A.; Scacchetti, M. Gem-quality morganite from Monte Capanne pluton (Elba Island, Italy). *Neues Jahrb. Miner. Abhandl.* **2016**, *1993*, 69–78. [[CrossRef](#)]
80. Morgan, G.B.; London, D. Alteration of amphibolitic wallrocks around the Tanco rare-element pegmatite, Bernic Lake, Manitoba. *Am. Mineral.* **1987**, *72*, 1097–1121.
81. Fan, Z.-W.; Xiong, Y.-Q.; Shao, Y.-J.; Wen, C.-H. Textural and chemical characteristics of beryl from the Baishawo Be-Li-Nb-Ta pegmatite deposit, Jiangnan Orogen: Implication for rare metal pegmatite genesis. *Ore Geol. Rev.* **2022**, *149*, 105094. [[CrossRef](#)]
82. Lum, J.E.; Viljoen, F.; Cairncross, B.; Frei, D. Mineralogical and geochemical characteristics of beryl (aquamarine) from the Erongo Volcanic complex, Namibia. *J. Afr. Earth Sci.* **2016**, *124*, 104–125. [[CrossRef](#)]
83. London, D. Ore-forming processes within granitic pegmatites. *Ore Geol. Rev.* **2018**, *101*, 349–383. [[CrossRef](#)]
84. Černý, P. Rare-element granitic pegmatites. Part 1: Anatomy and internal evolution of pegmatite deposits. *Geosci. Can.* **1991**, *18*, 49–67.
85. Trueman, D.L.; Černý, P. Exploration for rare-element granitic pegmatites. In *Proceedings of the Short Course in Granitic Pegmatites in Science and Industry*, Winnipeg, MB, Canada, 13–16 May 1982; Mineralogical Association of Canada: Quebec, QC, Canada, 1982; pp. 463–493.

**Disclaimer/Publisher’s Note:** The statements, opinions and data contained in all publications are solely those of the individual author(s) and contributor(s) and not of MDPI and/or the editor(s). MDPI and/or the editor(s) disclaim responsibility for any injury to people or property resulting from any ideas, methods, instructions or products referred to in the content.